

Shell effect on fission fragment mass distribution at E_{cn}^* up to 70 MeV: Role of multichance fission

S. Santra ^{1,2,*}, A. Pal ¹, D. Chattopadhyay,^{1,2,†} A. Kundu ^{1,2}, P. C. Rout,^{1,2} Ramandeep Gandhi ^{1,2}, A. Baishya ^{1,2}, T. Santhosh ^{1,2}, K. Ramachandran,¹ R. Tripathi ^{2,3}, B. J. Roy,¹ T. N. Nag,^{2,3} G. Mohanto,¹ S. De,^{1,2} B. K. Nayak ^{1,2} and S. Kailas ⁴

¹Nuclear Physics Division, Bhabha Atomic Research Centre, Mumbai 400085, India

²Homi Bhabha National Institute, Anushaktinagar, Mumbai 400094, India

³Radio Chemistry Division, Bhabha Atomic Research Centre, Mumbai 400085, India

⁴UM-DAE Centre for Excellence in Basic Sciences, Mumbai University, Mumbai 400098, India



(Received 25 April 2023; accepted 1 June 2023; published 20 June 2023)

Mass distributions of fission fragments produced from the ^{249}Bk compound nucleus (CN), populated by complete fusion of ^{11}B with ^{238}U , were measured for the excitation energies in the range of $E_{\text{cn}}^* \approx 36.7$ – 69.7 MeV. Nearly flat tops observed for these distributions indicate the presence of asymmetric fission, contrary to the pure Gaussian mass distributions expected at such high excitation energies. A fit to the mass distribution using three Gaussian functions provides an estimate of individual contributions from symmetric and asymmetric modes of fission. A significant contribution of the asymmetric component observed at CN excitation energies above 40 MeV can be understood only by invoking “multichance fission” in the calculations using the semiempirical model code GEF. A systematic analysis of the mass distributions for several heavy transuranic nuclei reveals that the manifestation of the fragment shell effect in the integral mass distributions are visible even up to an initial compound nucleus excitation of $E_{\text{cn}}^* \approx 70$ MeV due to their influence on the distributions of higher chance fissions.

DOI: [10.1103/PhysRevC.107.L061601](https://doi.org/10.1103/PhysRevC.107.L061601)

The dynamics of nuclear fission can be explained on the basis of the potential energy surface which is built using a macroscopic-microscopic model [1]. The macroscopic potential energy is obtained from the liquid drop (LD) model [2] and the microscopic shell and pairing correction energy is obtained using Strutinsky’s prescription [3]. Though the LD model has been very successful in explaining nuclear fission [2], it fails to predict the asymmetric mass distribution of fission fragments (FFs). The addition of the shell effect [4] to the LD model is not only able to explain the asymmetric nature of fission but also explains several other phenomena, such as the stability of many transuranium nuclei and long-lived superheavy elements (SHE) with Z beyond 104 for which the fission barrier vanishes [5,6], fission isomers [7], superdeformed nuclei [8], new magic numbers [9], etc. However, the shell effect on the fission mechanism is expected to wash out at higher compound nucleus excitation energies (E_{cn}^*) [10], where the probabilities of formation and survival of the transuranium and superheavy elements are very different from low excitation energies. Understanding of fission at high excitation energies is also important for nuclear-data evaluations related to the incineration and/or transmutation of the long-lived minor actinides into shorter-lived fission products

using high energy spallation neutrons. Thus, it is important to understand the fission process both at low as well as high excitation energies and particularly the upper limit of the initial compound nucleus (CN) excitation energy where the shell effect starts disappearing.

A few measurements on the CN excitation energy dependence of the shell effect on fission fragment mass distributions involving actinide targets exist in the literature, providing different values on the limit of E_{cn}^* . For instance, the study by Chaudhuri *et al.* [11] on α -induced reactions on a ^{232}Th target shows that the asymmetric nature of mass distribution vanishes at the excitation energy of ≈ 43 MeV, whereas in a recent study by Hirose *et al.* [12] the signature of asymmetric fission was observed up to $E_{\text{cn}}^* = 60$ MeV. However, the data of the second study suffer from poor statistics and large bin size (10 MeV) of excitation energy as the composite nuclei were populated by multinucleon transfer reactions with cross sections much smaller than complete fusion. On the other hand, due to the use of a very thick (1.1 mg/cm^2) target in Ref. [11] the uncertainties in the measurement of fragment velocities increase, which in turn lead to larger uncertainties in the mass distributions. In one of the measurements of fission of ^{250}Cf , populated by the $^{238}\text{U} + ^{12}\text{C}$ reaction [13], the signatures of shell effect on fragments at scission were observed at $E_{\text{cn}}^* = 45$ MeV. In another measurement on fission fragment mass distribution for the compound nucleus ^{242}Pu by Back *et al.* [14], it was observed that the shell effect persists certainly beyond 50 MeV of initial CN excitation energy,

*ssantra@barc.gov.in

[†]Present address: Department of Physics, The ICFAI University Tripura, West Tripura-799210, India.

although the exact value of the maximum limit on E_{cn}^* could not be obtained due to the lack of experimental data at higher excitation energies. Therefore, systematic measurements over a broad range of excitation energies are very important for the study of the excitation energy dependence of the shell effect. Second, to obtain precision experimental data on FF mass distribution with good statistics and well defined excitation energies with minimal target effect, one should populate the compound nucleus using a complete fusion reaction and a thin target, respectively.

The fission fragment mass distribution for actinides, at low excitation energies, is found to be predominantly asymmetric due to the strong shell effect in the formation of fragment nuclei. With increasing excitation energy, the gradual disappearance of the shell effect leads to an enhancement of the symmetric component and a reduction of the peak-to-valley (P:V) ratio in FF mass distributions [12,15–19]. Interestingly, with increasing excitation energy, the probability of consecutive neutron evaporation followed by fission of the residual composite nuclei, commonly known as multichance fission (MCF), becomes significant. The presence of MCF reduces the excitation energy of the residual composite nuclei at every step of chance fissions, leading to the reappearance of a stronger shell effect even though the excitation energy of the populated compound nucleus is much higher. In one of the early works, strong evidence of MCF was observed by Jensen *et al.* [20] and Perry *et al.* [21] in the fission fragment mass distribution measured in proton and deuteron induced reactions with ^{226}Ra . The concept of MCF is also well known from the studies of the fission probability in high-energy neutron-induced reactions. Recently, the role of multichance fission in the description of FF mass distributions [12,22] from actinide nuclei was explored. A few theoretical studies incorporating the effect of MCF on FF mass distributions are also available in the literature [23–28]. However, the lack of experimental data on the FF mass distribution for different compound nuclei at high excitation energies makes it difficult to validate the above theoretical models.

In this Letter, the results of FF mass distributions for heavy actinide nuclei ^{249}Bk populated by the $^{11}\text{B} + ^{238}\text{U}$ reaction at higher excitation energies are discussed. The role of MCFs is explored in the measured mass distributions by comparing them with the predictions from the widely used semiempirical code GEF [25,29]. We make a systematic analysis of the relative contributions of symmetric and asymmetric fission modes [11] for several heavy transuranic nuclei available in the literature along with the present experimental data to find the maximum CN excitation energies up to which the shell effect on mass distribution may persist.

Two sets of experiments were carried out on the $^{11}\text{B} + ^{238}\text{U}$ reaction at the 14-UD BARC-TIFR Pelletron-Linac facility, Mumbai, using pulsed beam with energies $E_{\text{beam}} = 53.0\text{--}65.0$ MeV (from Pelletron) and then with $E_{\text{beam}} = 69.1\text{--}87.4$ MeV (from Pelletron+LINAC). A ^{238}U target of thickness $\approx 100\ \mu\text{g}/\text{cm}^2$, sandwiched between two layers of ^{12}C of thickness $\approx 15\ \mu\text{g}/\text{cm}^2$ each, was used. Two position sensitive multiwire proportional counters (MWPCs) [30] were placed symmetrically on either side of the beam at the folding angles, each at a distance of about 40 cm

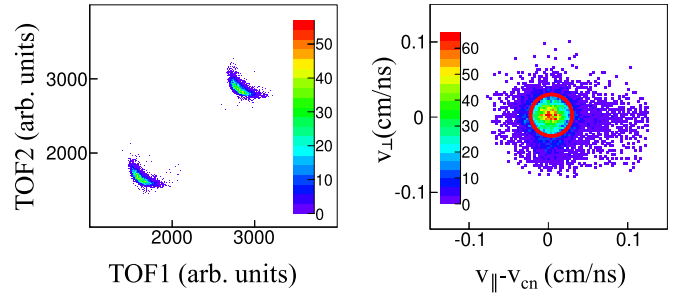


FIG. 1. (a) Typical correlation of time of flight of both the fission fragments, cleanly identifying the binary events. Two banana-shaped spectra correspond to two different beam bunches. (b) Typical $v_{\perp} - v_{cn}$ versus v_{\parallel} plot and the red contour corresponding to the binary events following the complete fusion process forming the nucleus ^{249}Bk at 58 MeV projectile energy.

from the target center to detect the coincident fission fragments. The timing correlation spectrum of the two particles detected in coincidence, as shown in Fig. 1(a), provides a clean separation of the fission fragments from elastic or quasielastic events. The position and timing of the spectra were calibrated following the procedure given in Ref. [30]. The time zero was obtained by fulfilling the criteria [31,32] that (i) the parallel component of the velocity vector of the fissioning nucleus should be peaking at the velocity equal to the velocity of the compound nucleus, (ii) the perpendicular component of the velocity vector of the fissioning nucleus should be peaking at zero, and (iii) the mass distribution which is obtained by taking the ratio of FF velocities (v_{1cm}, v_{2cm}) in the center of mass frame should be symmetric around half of the mass of the compound nucleus ^{249}Bk (though a slight shift towards the left is expected due to MCF contributions, but is invisible due to limited mass resolution and would not affect present conclusions). Energy loss in the target and backing medium was calculated using SRIM [33] and was taken into account in the above analysis.

A correlation plot of parallel versus perpendicular components of velocity vectors (v_{\parallel} vs v_{\perp}), helpful to reject the contribution of transfer fission [34] and obtain the FF mass and TKE distribution corresponding to pure complete fusion process, was generated. In the case of complete fusion, v_{\parallel} of the fissioning nucleus should be equal to the velocity of the compound nucleus v_{cn} and v_{\perp} should be equal to zero. A typical v_{\perp} versus $v_{\parallel} - v_{cn}$ plot is shown in Fig. 1(b) for 58 MeV beam energy, where an intense peak corresponding to complete fusion events is observed around the (0,0) coordinate as expected, indicating the accuracy of the timing calibration obtained in the present measurement. Note that only the intense events within the red circle of radius ≈ 0.02 cm/ns, assumed to be due to the binary fission of the compound nuclei of ^{249}Bk , were analyzed to derive the mass and total kinetic energy (TKE) distributions. The scattered events surrounding the red circle are dominated by the transfer induced fission events.

The measured velocities of the fission fragments were used in a two-body kinematics to determine the masses and kinetic

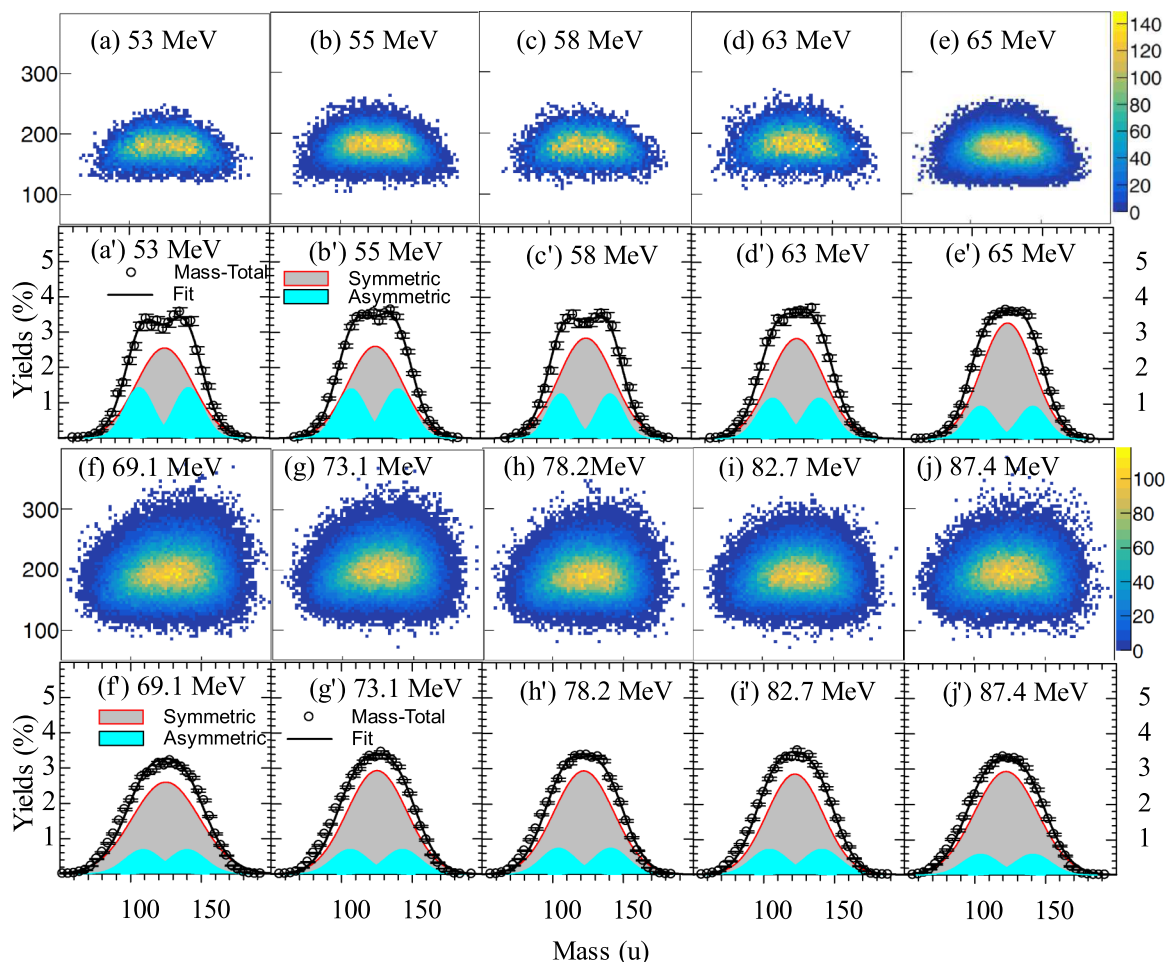


FIG. 2. (a)–(e), (f)–(j) Mass-TKE correlations at different beam energies. (a')–(e'), (f')–(j') Projections of respective two-dimensional plots onto the mass axis and their fits using multiple Gaussian functions (grey and cyan filled areas).

energies of the fragments on event-by-event basis, assuming the sum of the projectile and target masses to be equal to the compound nuclear mass. The mass-TKE correlation plots obtained for different beam energies are shown in Figs. 2(a)–2(j). Due to strong competition between the asymmetric and symmetric superlong modes [35] it is difficult to cleanly identify these two modes from the above plots. The TKE distributions obtained from the projections of Figs. 2(a)–2(j) on the y axis for all the measured energies (not shown here) are found to be Gaussians peaking around 178 MeV, consistent with the Viola systematics [36]. However, the corresponding mass distributions, i.e., projections of Figs. 2(a)–2(j) on x axis, shown as open circles in 2(a')–2(j'), are not perfect Gaussians. At low beam energies, the distributions are either double peaked or have flat tops. One of the peaks observed around $A \approx 140$ confirms the presence of asymmetric fission which is in strong competition with the symmetric mode described by the LD model. In order to find out the contribution from each modes, the measured distributions were fitted using three Gaussian functions corresponding to one symmetric component (grey filled area) and two asymmetric components (cyan filled areas) as shown in Figs. 2(a')–2(j'). The extracted ratio of asymmetric to symmetric contributions, as shown in Fig. 3,

is found to decrease with the increase in E_{cn}^* , as expected. However, it is interesting to see that the value of the ratio is significant even up to an E_{cn}^* of 70 MeV.

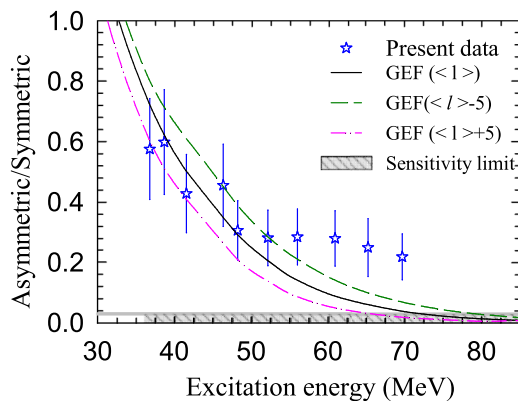


FIG. 3. Ratio of asymmetric to symmetric contributions (stars) obtained from experimental mass distributions in the fission of ^{249}Bk compared with the GEF predictions using different angular momenta (lines). The hatched area near the x axis represents region of insensitivity of present measurement.

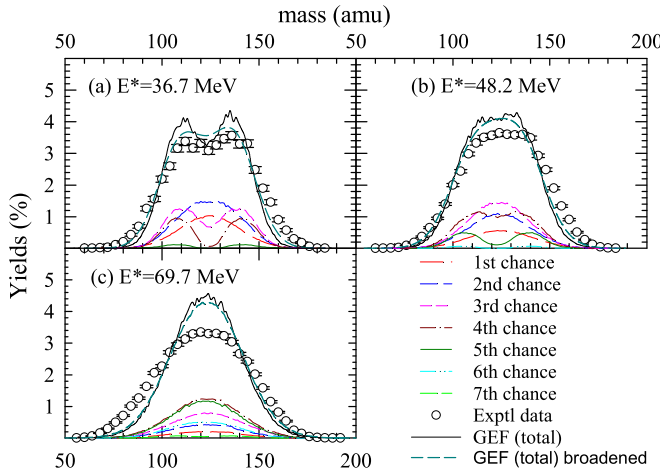


FIG. 4. Comparison of typical experimental FF mass distributions at CN (^{249}Bk) excitation energies of (a) 36.7, (b) 48.2 and (c) 69.7 MeV with the GEF calculations (solid lines) including contributions from individual chance fissions (broken lines). Short-dashed dark cyan lines represent GEF calculations broadened by experimental mass resolution with $\sigma = 6$ u.

From different theoretical model calculations, the shell effect is predicted to wash out at an excitation energy ≈ 40 MeV [37,38]. Thus the presence of an asymmetric mode observed at such high energies may actually be due to the reduced effective excitation energies (E_{eff}^*) of the fissioning nuclei. This can be understood in terms of multichance fission (MCF) where neutrons successively get evaporated from the compound nucleus, thereby reducing E_{eff}^* of the residual composite nuclei. There is a finite probability of neutron evaporation from the compound nucleus at each step of the MCF process which depends on its initial excitation energy. In each step, the mass distribution is different due to a change in excitation energy. Therefore, model calculations must combine the mass distributions calculated for every steps of MCF (first chance, second chance, third chance, etc.) weighted with respective chance probabilities to explain the experimental data.

The semiempirical model code GEF [25,29] was used to calculate the mass distributions for different chance fission as shown by different lines in Figs. 4(a)–4(c). The average angular momenta (ℓ) required for the above calculations were obtained from the coupled channels calculations using CCDEF [39]. It can be observed that for all energies the calculated mass distributions corresponding to the first chance-fission are symmetric and cannot explain the experimental mass distributions. However, the presence of MCF up to seventh chance with varying probabilities with E_{cn}^* has introduced the asymmetric components. The sum total of mass distributions weighted over different chance fission, shown by the black solid lines in Figs. 4(a)–4(c), provides a reasonable agreement with the overall behavior of the measured mass distributions for three typical excitation energies of 36.7, 48.2, and 69.7 MeV respectively. Due to the limitation in experimental mass resolution with $\sigma_m \approx 6$ u, the above calculated distributions are expected to broaden which was simulated by

broadening each distribution point with a Gaussian distribution. The results of the broadened theoretical distributions are shown as short-dashed dark cyan lines which are slightly closer to the experimental mass distributions.

The GEF calculations were extended further for a wide range of excitation energies (25–85 MeV) to not only compare with the measured data at remaining energies but also estimate the highest value of E_{cn}^* where the shell effect washes out after incorporating the effect of multichance fission. The contributions for symmetric and asymmetric components in the total mass distributions were calculated at each CN excitation energy by adding the weighted contributions from all possible chances. The respective ratio of asymmetric to symmetric contributions calculated for different excitation energies (represented by a solid line) shows a trend consistent with the ones obtained from the fitting of the measured mass distribution using multiple Gaussian functions (represented by stars) as compared in Fig. 3. Interestingly, one can observe that the predicted contribution from the asymmetric mode for $E_{\text{cn}}^* \approx 70$ MeV enters below the sensitivity of the present experiment, which is around the 3% level as shown by the hatched region near the x axis of Fig. 3. The GEF predictions for individual chance fission at $E_{\text{cn}}^* = 69.7$ MeV, as shown in Fig. 4(c), reveal that the maximum contribution to total fission comes from the fourth chance. Second, the fission modes for most of the orders of chance fissions are symmetric. Therefore, one can understand that the shell effect, that leads to asymmetric modes of fission in $^{11}\text{B} + ^{238}\text{U}$, disappears when the initial CN excitation energy $E_{\text{cn}}^* \approx 70$ MeV, which is much higher than the results reported in Ref. [11] for fission in $\alpha + ^{232}\text{Th}$.

To see the sensitivity of the above results on angular momenta populated with the CN, the GEF calculations were repeated with two additional angular momenta with values on either side of the average angular momentum, i.e., $\ell = \langle \ell \rangle - 5\hbar$ and $\ell = \langle \ell \rangle + 5\hbar$ at each excitation energy, and the results are shown as dashed (green) and dot-dashed (pink) lines respectively in Fig. 3. It is interesting to note that the contribution of the asymmetric mode of fission increases with the decrease in the value of ℓ , and if the same compound nucleus could be populated with similar excitation energy but angular momentum $\ell = \langle \ell \rangle - 5\hbar$ then the contribution from the asymmetric component due to the shell effect can persist even up to $E_{\text{cn}}^* = 80$ MeV. This is a consequence of the fact that lower ℓ favors fission survival, thus increasing the contribution from higher chance fission [22].

In order to confirm the above observation on excitation energy dependence of the shell effect in the fission of the present compound nucleus ^{249}Bk , a systematic study was made using the experimental data available in the literature for several heavy actinides such as ^{241}Np [12], ^{242}Pu [12,14], ^{247}Cf [22], and ^{250}Cf [40] along with the present data (^{249}Bk) and comparing their experimental mass distributions with the GEF predictions. Similarly to ^{249}Bk , the contributions of asymmetric fission were extracted for the above nuclei by fitting their experimental mass distributions by triple Gaussian functions (not shown here). The percentage contributions from asymmetric fission modes for different compound nuclei along with the present data are represented by different

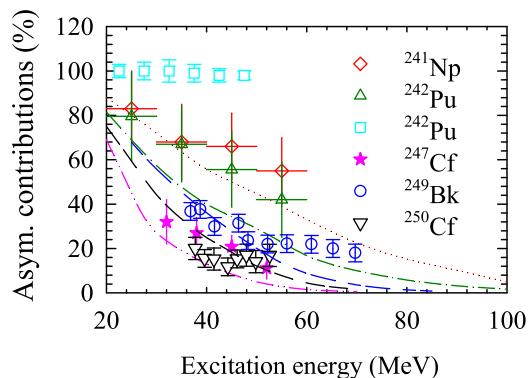


FIG. 5. Systematics on the excitation energy dependence of asymmetric fission contribution (symbols) extracted from existing experimental mass distributions for ^{241}Np [12], ^{242}Pu (triangles [12]), ^{242}Pu (squares [14]), ^{247}Cf [22], and ^{250}Cf [40] along with the present data for ^{249}Bk compared with the GEF predictions represented by dotted, dot-dashed, dot-dot-dashed, dashed, and short-long-dashed lines respectively.

symbols in Fig. 5, which are compared with the respective predictions using GEF as represented by matching color lines. It may be observed that the overall trend for the excitation energy dependence of the percentage asymmetric fission contribution is similar for most of the experimental data and is consistent with the GEF predictions. It is surprising to find the data on ^{242}Pu (squares) by Back *et al.* to be inconsistent with the GEF prediction and completely different from the data (triangles) for the same compound nucleus formed through a different entrance channel. It may also be noted that the data for ^{241}Np and ^{242}Pu [12] are associated with large errors because they were populated by transfer reactions with less statistics and their values are systematically higher than the calculations. However, all of them agree with the fact that the initial CN excitation energy for which the manifestation of the shell effect on the integral mass distribution vanishes is much higher than one would normally expect. It may also be observed that, for a particular excitation, the asymmetric contribution systematically decreases from lighter to heavier compound nuclei, which could be due to the decrease in the fission barrier, leading to enhanced symmetric fission contributions.

In summary, mass distributions of fission fragments of ^{249}Bk nuclei, populated by the $^{11}\text{B} + ^{238}\text{U}$ reaction, were measured at $E_{\text{cn}}^* = 36.7\text{--}69.7$ MeV. The mass-TKE correlation plots show a strong competition between asymmetric

and symmetric modes of fission for most of the excitation energies. The percentage contributions for asymmetric and symmetric modes were extracted by fitting the measured mass distributions using three appropriately described Gaussian distributions. The contribution from the symmetric (asymmetric) mode is found to increase (decrease) with the increase in the excitation energy, as expected. However, for such high excitation energies, the measured mass distributions are expected to be predominantly symmetric unless we invoke the concept of multichance fission. Hence, theoretical model calculations using GEF code were performed incorporating multichance fission. The first-chance fission is found to be predominantly symmetric at all the measured initial excitation energies, whereas the asymmetric mode comes into play only at higher-chance fissions. Therefore first-chance fission alone cannot explain the nature of measured mass distributions. The model calculations, taking into account the multichance fissions with appropriate weight factors, could explain the experimental mass distribution data as well as the relative contributions of symmetric and asymmetric modes at different excitation energies reasonably well.

The excitation energy dependence of the asymmetric component of the total fission of ^{249}Bk reveals that the maximum initial CN excitation energy E_{cn}^* up to which the shell effect on the integral mass distribution is manifested can be as high as 70 MeV, consistent with the observation of Ref. [12] and contrary to the much lower limit of 43 MeV reported in Ref. [11]. A systematics on the excitation energy dependence of the asymmetric component of fission of several transuranic nuclei along with ^{249}Bk was made using the available experimental data on fission fragment mass distribution and corresponding theoretical model calculations. The study confirms that the initial CN excitation energy beyond which the manifestation of the shell effect on the integral FF mass distribution for most of these nuclei diminishes is ≈ 70 MeV, albeit with an uncertainty depending on the angular momentum of the CN. Thus, the present work confirms the role of multichance fission in the description of FF mass distributions from heavier actinide nuclei, and the reported high limits of initial compound nucleus excitation energies beyond which the shell effect vanishes are expected to have important implications in the study of SHE synthesis.

We thank K.-H. Schmidt, C. Schmitt, and K. Mahata for helpful discussions during the preparation of the manuscript. One of the authors (S.K.) acknowledges INSA for support from a senior scientist fellowship.

[1] K. H. Schmidt and B. Jurado, *Rep. Prog. Phys.* **81**, 106301 (2018).
 [2] N. Bohr and J. Wheeler, *Phys. Rev.* **56**, 426 (1939).
 [3] V. M. Strutinsky, *Nucl. Phys. A* **95**, 420 (1967).
 [4] Maria G. Mayer, *Phys. Rev.* **74**, 235 (1948).
 [5] Y. T. Oganessian and V. K. Utyonkov, *Rep. Prog. Phys.* **78**, 036301 (2015).

[6] S. A. Giuliani, Z. Matheson, W. Nazarewicz, E. Olsen, P.-G. Reinhard, J. Sadhukhan, B. Schuetrumpf, N. Schunck, and P. Schwerdtfeger, *Rev. Mod. Phys.* **91**, 011001 (2019).
 [7] V. M. Strutinsky, *Nucl. Phys. A* **122**, 1 (1968).
 [8] R. V. F. Janssens and T. L. Khoo, *Annu. Rev. Nucl. Part. Sci.* **41**, 321 (1991).

- [9] R. Kanungo, C. Nociforo, A. Prochazka, T. Aumann, D. Boutin, D. Cortina-Gil, B. Davids, M. Diakaki, F. Farinon, H. Geissel, R. Gernhauser, J. Gerl, R. Janik, B. Jonson, B. Kindler, R. Knobel, R. Krucken, M. Lantz, H. Lenske, Y. Litvinov *et al.*, *Phys. Rev. Lett.* **102**, 152501 (2009).
- [10] R. Vandenbosch and J. R. Huizenga, *Nuclear Fission* (Academic, New York, 1973).
- [11] A. Chaudhuri, T. K. Ghosh, K. Banerjee, S. Bhattacharya, J. Sadhukhan, C. Bhattacharya, S. Kundu, J. K. Meena, G. Mukherjee, R. Pandey *et al.*, *Phys. Rev. C* **91**, 044620 (2015).
- [12] K. Hirose, K. Nishio, S. Tanaka, R. Leguillon, H. Makii, I. Nishinaka, R. Orlandi, K. Tsukada, J. Smallcombe, M. J. Vermeulen *et al.*, *Phys. Rev. Lett.* **119**, 222501 (2017).
- [13] M. Caamaño, O. Delaune, F. Farget, X. Derkx, K.-H. Schmidt, L. Audouin, C.-O. Bacri, G. Barreau, J. Benlliure, E. Casarejos *et al.*, *Phys. Rev. C* **88**, 024605 (2013).
- [14] B. B. Back, A. C. Shotter, T. J. M. Symons, A. Bice, C. K. Gelbke, T. C. Awes, and D. K. Scott, *Phys. Rev. C* **23**, 1105 (1981).
- [15] I. Itkis, A. Bogachev, A. Chizhov, D. Gorodisskiy, M. Itkis, G. Knyazheva, N. Kondratiev, E. Kozulin, L. Krupa, S. Mulgin, I. Pokrovsky, E. Prokhorova, A. Rusanov, V. Voskressenski, and S. Zhdanov, *Phys. Lett. B* **640**, 23 (2006).
- [16] S. Santra, A. Pal, P. K. Rath, B. K. Nayak, N. L. Singh, D. Chattopadhyay, B. R. Behera, V. Singh, A. Jhingan, P. Sugathan, K. S. Golda, S. Sodaye, S. Appannababu, E. Prasad, and S. Kailas, *Phys. Rev. C* **90**, 064620 (2014).
- [17] R. Léguillon, K. Nishio, K. Hirose, H. Maki, I. Nishinaka, R. Orlandi, K. Tsukada, J. Smallcombe, S. Chiba, Y. Aritomoto, T. Ohtsuki, R. Tatsuzawa, N. Takaki, N. Tamura, S. Goto, I. Tsekhanovich, C. M. Petrachi, and A. N. Andreyev, *Phys. Lett. B* **761**, 125 (2016).
- [18] A. Pal, S. Santra, D. Chattopadhyay, A. Kundu, A. Jhingan, P. Sugathan, N. Saneesh, M. Kumar, N. L. Singh, A. Yadav, C. Yadav, R. Dubey, K. Kapoor, K. Rani, H. Arora, A. C. Visakh, D. Kaur, B. K. Nayak, A. Saxena, S. Kailas, and K. H. Schmidt, *Phys. Rev. C* **98**, 031601(R) (2018).
- [19] A. Pal, S. Santra, P. C. Rout, R. Gandhi, A. Baishya, T. Santhosh, R. Tripathi, and T. N. Nag, *Phys. Rev. C* **104**, L031602 (2021).
- [20] R. C. Jensen and A. W. Fairhall, *Phys. Rev.* **118**, 771 (1960).
- [21] D. G. Perry and A. W. Fairhall, *Phys. Rev. C* **4**, 977 (1971).
- [22] J. Khuyagbaatar, D. J. Hinde, I. P. Carter, M. Dasgupta, C. E. Dullmann, M. Evers, D. H. Luong, R. du Rietz, A. Wakhle, E. Williams, and A. Yakushev, *Phys. Rev. C* **91**, 054608 (2015).
- [23] M. C. Duijvestijn, A. J. Koning, and F.-J. Hamsch, *Phys. Rev. C* **64**, 014607 (2001).
- [24] M. D. Usang, F. A. Ivanyuk, C. Ishizuka, and S. Chiba, *Phys. Rev. C* **94**, 044602 (2016).
- [25] K.-H. Schmidt, B. Jurado, C. Amouroux, and C. Schmitt, *Nucl. Data Sheets* **131**, 107 (2016).
- [26] P. Möller and C. Schmitt, *Eur. Phys. J. A* **53**, 7 (2017).
- [27] H. Paşca, A. Andreev, G. Adamian, and N. Antonenko, *Eur. Phys. J. A* **54**, 104 (2018).
- [28] S. Tanaka, Y. Aritomo, Y. Miyamoto, K. Hirose, and K. Nishio, *Phys. Rev. C* **100**, 064605 (2019).
- [29] B. Jurado and K. H. Schmidt, Computer code GEF, Version 1.2, 2020, <http://www.cenbg.in2p3.fr/GEF>.
- [30] A. Pal, S. Santra, A. Kundu, D. Chattopadhyay, A. Jhingan, B. Nayak, and S. Prafulla, *J. Instrum.* **15**, P02008 (2020).
- [31] R. G. Thomas, D. J. Hinde, D. Duniec, F. Zenke, M. Dasgupta, M. L. Brown, M. Evers, L. R. Gasques, M. D. Rodriguez, and A. Diaz-Torres, *Phys. Rev. C* **77**, 034610 (2008).
- [32] R. Rafiei, R. G. Thomas, D. J. Hinde, M. Dasgupta, C. R. Morton, L. R. Gasques, M. L. Brown, and M. D. Rodriguez, *Phys. Rev. C* **77**, 024606 (2008).
- [33] J. Ziegler, Computer code SRIM, 2013, <http://www.srim.org/>.
- [34] D. J. Hinde, M. Dasgupta, J. R. Leigh, J. P. Lestone, J. C. Mein, C. R. Morton, J. O. Newton, and H. Timmers, *Phys. Rev. Lett.* **74**, 1295 (1995).
- [35] M. D. Usang, F. A. Ivanyuk, C. Ishizuka, and S. Chiba, *Sci. Rep.* **9**, 1525 (2019).
- [36] V. E. Viola, K. Kwiatkowski, and M. Walker, *Phys. Rev. C* **31**, 1550 (1985).
- [37] S. S. Kapoor and V. S. Ramamurthy, *Pramana - J. Phys.* **5**, 124 (1975).
- [38] S. S. Kapoor, *Pramana - J. Phys.* **59**, 941 (2002).
- [39] J. Fernandez-Niello, C. H. Dasso, and S. Landowne, *Comput. Phys. Commun.* **54**, 409 (1989).
- [40] C. Yadav *et al.*, *Phys. Rev. C* **86**, 034606 (2012).